Tumor-immune signatures of treatment resistance to brentuximab vedotin with ipilimumab and/or nivolumab in Hodgkin lymphoma

Edgar Gonzalez-Kozlova[1,2,3], Hsin-Hui Huang[4], Opeyemi A. Jagede[5], Kevin Tuballes[1], Diane M. Del Valle[1], Geoffrey Kelly[6], Manishkumar Patel[6], Hui Xie[6], Jocelyn Harris[6], Kimberly Argueta[6], Kai Nie[6], Vanessa Barcessat[1], Radim Moravec[7], Jennifer Altreuter[5,8], Dzifa Y. Duose[9], Brad S. Kahl[10], Stephen M. Ansell[11], Joyce Yu[5], Ethan Cerami[5,8], James R. Lindsay[5,8], Ignacio I. Wistuba[9], Seunghee Kim-Schulze[1,2,3,6], Catherine S. Diefenbach[12$], Sacha Gnjatic[1,2,3,6$#]

[1]Department of Oncological Sciences, [2]Tisch Cancer Institute, [3]Precision Immunology Institute, [4]Department of Population Health Science and Policy, [6]Human Immune Monitoring Center, Icahn School of Medicine at Mount Sinai, New York, NY
[5]Department of Data Science, [8]CIMAC-CIDC Network, Pipeline development and Portal integration, Dana-Farber Cancer Institute, Boston, MA
[7]Cancer Therapy Evaluation Program, Division of Cancer Treatment and Diagnosis, NCI, Bethesda, MD.
[9]Department of Translational Molecular Pathology, The University of Texas MD Anderson Cancer Center, Houston, TX
[10]Washington University School of Medicine
[11]Mayo Clinic
[12]Perlmutter Cancer Center, NYU Langone Health, New York, NY

$ Equal contribution
# Corresponding author

Mailing address: Icahn School of Medicine at Mount Sinai, 1470 Madison Avenue, Hess s5-105, Box 1044A, New York NY 10029
Phone: (212) 824-8438
Email address: sacha.gnjatic@mssm.edu, edgar.gonzalez-kozlova@mssm.edu

Running title: Hodgkin lymphoma immunotherapy resistance signatures

Keywords: Multi-omics, immune checkpoint inhibitors, immunotherapy, translational study, biomarkers, relapse/refractory Hodgkin lymphoma, proteomics, phenotyping

mailing address, email address, and phone number
Please correct the issue and upload a new version of the manuscript file.

Conflict-of-interest disclosure

S.G. reports other research funding from Boehringer-Ingelheim, Bristol-Myers Squibb, Celgene, Genentech, Regeneron, and Takeda. CD reports research funding from Bristol-Myers Squibb, Merck, and Seattle Genetics.

Abstract

Purpose: To investigate the cellular and molecular mechanisms associated with targeting CD30-expressing Hodgkin Lymphoma (HL) and immune checkpoint modulation induced by combination therapies of CTLA-4 and PD1.

Patients and Methods: Phase 1/2, multicenter, open-label, trial NCT01896999 enrolled patients with refractory or relapsed HL (R/R HL) after one or more lines of therapy, with adequate performance status and organ function. Using peripheral blood, we assessed soluble proteins, cell composition, T cell clonality, and tumor antigen-specific antibodies in 54 patients enrolled in the phase 1 component of the trial.

Results: NCT01896999 reported high (>75%) overall objective response rates with brentuximab-vedotin (BV) in combination with ipilimumab (I) and/or nivolumab (N) in patients with R/R HL. We observed durable increase in soluble PD-1 and plasmacytoid dendritic cells as well as decreases in plasma CCL17, ANGPT2, MMP12, IL13, and CXCL13 in N-containing regimens (BV+N and BV+I+N) compared with BV+I ($p<0.05$). Non-responders and patients with short progression free-survival showed elevated CXCL9, CXCL13, CD5, CCL17, adenosine-deaminase, and MUC16 at baseline or after one treatment cycle and a higher prevalence of NY-ESO-1-specific autoantibodies ($p<0.05$).

Conclusions: The results suggest a circulating tumor-immune-derived signature of BV±I+N treatment resistance that may be useful for patient stratification in combination checkpoint therapy.

Significance Statement

Identification of multi-omic immune markers from peripheral blood may help elucidate resistance mechanisms to checkpoint inhibitor and antibody drug conjugate combinations with potential implications for treatment decisions in relapsed HL.

Introduction

FDA-approved novel therapies have transformed the treatment options available for relapsed or refractory (R/R) Hodgkin lymphoma (HL). Brentuximab vedotin (BV), an anti-CD30 antibody-drug conjugate (ADC), was FDA approved in 2011 for R/R HL patients who have undergone autologous stem cell transplant (SCT) or multiple chemotherapy regimens, based on an CR rate of 34% and an overall duration of response of 5.6 months (20.5 mo in those with CR) (1). Subsequently, in 2016, the PD-1-targeting checkpoint inhibitors nivolumab and pembrolizumab were also approved for R/R HL. However, single agent nivolumab has a complete response (CR) rate of 14-16%, and a PFS of 15 months in patients with prior exposure to BV (2). In solid tumors, studies have shown that combining anti-CTLA-4 treatment (ipilimumab) with PD-1 blockade (nivolumab or pembrolizumab) can improve response rates in diverse types of tumors, at the cost of a higher rate of adverse events. (3,4).

The phase 1/2 study E4412 (NCT01896999) evaluated the safety and efficacy of single or dual checkpoint blockade with ipilimumab (I) and/or nivolumab (N) in R/R HL in combination with the antibody drug conjugate BV (5). This combination was hypothesized to deplete CD30-

expressing Hodgkin and Reed/Sternberg (HRS) cells and to activate T effector cells to target HRS cell killing and overcome therapeutic resistance. We reported a CR rate of 57% (95% CI 34–78%) for BV+I, 61% (36–83%) for BV+N, and 73% (50–89%) for BV+I+N arms (5). An increased number of grade 3-4 adverse events was associated with treatment arms that included ipilimumab (43-55%) as compared to the BV+N arms (21%). These promising results prompted an expansion to the planned phase 2 of this trial with a randomized comparison of BV+N vs. BV+I+N, which recently completed adult enrollment. Molecular and cellular immune profiling of biomarkers that could explain differential response or survival to these ADC and CPI combinations has not been described to date.

To identify immune mechanisms associated with BV+I±N immunotherapy and biomarkers of resistance or adverse events, which could guide future treatment decisions, we applied longitudinal immune monitoring and analysis of blood specimens collected during phase 1 throughout the course of treatment. Using cellular and molecular multi-omics, we examined peripheral markers for associations with clinical outcomes. We performed four different assays using peripheral blood plasma and mononuclear cells on specimens collected from 54 patients from the phase 1 component of this trial (19 in the BV+I group, 16 in the BV+N group, and 19 in the triplet group) (5) including: 1) Olink proximity extension assay (PEA) to detect 92 soluble protein plasma analytes, 2) ELISA Grand Serology to measure circulating plasma antibody titers against 20+ known tumor antigens, 3) Mass cytometry CyTOF to assess peripheral blood cell composition, and cell surface activation/inhibitory marker expression; and 4) Bulk Vβ TCR-seq to quantify T-cell immune repertoire diversity. Data from these assays was correlated to response rate (categorical, from imaging data, best achieved) and survival (for predictions at baseline only).

Materials and Methods

Clinical trial and biospecimens

This clinical trial started with Phase 1 and is currently completing Phase 2 (ClinicalTrials.gov Identifier: NCT01896999). Patient characteristics, including demographics, previous lines of treatment, as well as safety and preliminary efficacy are described in (5). During the dose escalation phase, three consecutive treatment groups were enrolled consisting of two arms receiving brentuximab vedotin 1.8 mg/kg q3w with ipilimumab at either 1 or 3 mg/kg q6w (BV+I, n=6 for Arm A, n=6 for Arm B); brentuximab vedotin at either 1.2 or 1.8 mg/kg q3w with nivolumab 3 mg/kg q3w (BV+N, n=3 for Arm D, n=6 for Arm E); and brentuximab vedotin at either 1.2 or 1.8 mg/kg q3w with nivolumab 3 mg/kg q3w and ipilimumab 1 mg/kg q12w (BV+I+N, n=7 for Arm G, n=5 for Arm H). Another 7 patients per treatment group were subsequently enrolled into expansion arms (arms C, F, and I) at the highest respective doses to establish safety and preliminary efficacy (Fig. 1A). For this correlative study, Arms A-C (BV+I), D-F (BV+N), and G-I (BV+N) were respectively combined, as no significant clinical difference was observed related to dose escalation. Blood (cryopreserved after separation as plasma and PBMCs) was collected prior to the start of treatment (baseline), on day 1 of cycle 2 [prior to drug infusion] (C2D1), at time of first restaging PET/CT [+/- 5 days] prior to cycle 4 (restaging) when clinical response was assessed, and after completion of therapy or off treatment (off study). The best objective response rate (BOR), including complete response (CR) and partial response (PR), at each respective time point, was determined using the International Harmonization

Project Group 2007 Revised Response Criteria according to Cheson and Deauville criteria as mandated by trial design (5). (RRID:SCR_001905, RRID:SCR_015654, RRID:SCR_006442)

Olink

Soluble protein analytes from peripheral blood plasma samples were quantified by Olink's proximity extension immunoassay platform using the Immuno-Oncology (IO) panel. This multiplex immunoassay allows the simultaneous measurement of 92 proteins, including cytokines, chemokines, and IO markers, across 96 plasma samples, including internal and external reference controls, and was performed following the manufacturer's instructions (https://cimac-network.org). The Olink data was normalized into NPX values (Normalized Protein eXpression) on a log2 scale (https://www.olink.com/question/what-is-npx/) (RRID:SCR_003899).

Grand serology

Enzyme-linked immunosorbent assay, ELISA, was used to detect and quantify circulating IgG antibodies to known tumor antigens, as previously described (6). Briefly, plasma samples were analyzed by low-volume semi-automated ELISA for seroreactivity to a panel of recombinant protein antigens (NY-ESO-1, P53, SOX2, HORMAD1, ERG, DHFR, PRAME, WT1, MELAN-A, SURVIVIN, UBTD2, CT47, MAGE-A4, SSX4, CT10, SSX2, XAGE, GAGE7 and MAGE-A10). Low-volume 96-well plates were coated overnight at 4°C with 0.5 µg/ml antigen and blocked for 2h at RT with PBS containing 5% non-fat milk and 0.1% Tween 20. Plasma was titrated from 1/100 to 1/6400 in 4-fold dilutions and added to blocked and washed 96-well plates. For assay validation and titer calculation, each plate contained positive and negative controls (pool of healthy donor sera). After overnight incubation, plates were extensively washed with PBS 0.2% Tween 20 and rinsed with PBS. Plasma antigen-specific IgG was detected after incubation with alkaline-phosphatase conjugated goat anti-human IgG (SouthernBiotech 2040-04, diluted 1/4,500), revelation using AttoPhos® substrate and buffer, and measurement using a fluorescence reader (BioTek Synergy). By linear regression, a reciprocal titer was calculated for each sample and for each antigen as the predicted or interpolated dilution value at which the titration curve meets a cutoff value (7). A positive significant result was defined as reciprocal titers > 100. (RRID:SCR_019873)

CyTOF

Mass cytometry using time of flight (CyTOF) analyses were performed on PBMCs using a harmonized protocol as described previously (8). Briefly, 1-5x10^6 thawed PBMCs were barcoded using palladium-based mass tags. Cells were then stained with a metal-conjugated antibody panel designed to characterize major immune subsets and surface activation markers, along with bead controls spiked-in for data normalization. FCS files underwent bead-based normalization, followed by exclusion of Ce140þ beads and bead-cell doublets, Gaussian ion cloud multiplet fusion events, and Rh103þ dead cells. Major immune-cell subsets were identified using hierarchical clustering approach (Astrolabe Diagnostics, Inc) and further confirmed using manual gating. The resulting tables contain cell number, cell frequency and marker expression quantiles. Data was transferred to R for differential abundance and surface marker expression analysis using orloj, lme4, dream and survival packages. (RRID:SCR_021055, RRID:SCR_019916, RRID:SCR_019917, RRID:SCR_021669). Panel of antibodies and reagents used for CyTOF are included as supplementary table 1.

TCR-seq

We used the immunoSEQ® Kit from the Adaptive Biotechnologies Corporation that targets T cell receptor beta chain (TCRβ) genes to enumerate rearranged TCRβ sequences in DNA isolated from PBMCs. The assay specifically targets the Complementarity Determining Region 3 (CDR3) of human TCRβ gene sequences, formed by rearrangement of the Variable (V), Diversity (D), and Joining (J) gene segments and including non-template Nucleotide (N) insertions and deletions at the gene segment junctions. Application of the immunoSEQ® Kit was analytically validated and performed by the MD Anderson Cancer Center CIMAC. The minimum DNA input for the assay was 200 ng per sample. Specifically, the DNA was processed with immunoSEQ hsTCRB kit (cat # ISK10050) and Illumina MiSeq Reagent Kit v3 to generate libraries and sequenced by Illumina MiSeq Sequencing system (150 cycles). The resulting FASTQ files were processed with the Immunarch pipeline to obtain individual clonal quantifications. The resulting data was analyzed using R, lme4, dream and survival packages. (RRID:SCR_014709)

Statistical Analysis

Quality controls. The analysis for all datasets (Olink, Serology, CyTOF, and TCRseq) was performed in R software using a mixed linear model strategy to adjust for relevant clinical variables and demographics. The data distributions for markers and cell populations for all assays were investigated as part of a routine quality control to identify biases, and corrected as follows: (1) samples with more than 50% missing values in any analyte were excluded; (2) Olink analytes that were under the limit of detection in more than 50% of samples were excluded; (3) CyTOF cell populations unassigned by Astrolabe were ignored. QC analyses were used to identify biases such as low detection and poor-quality samples.

Variance analysis. Sample variance profiles were performed to assess the effect of covariates with assay data (Olink, Serology, CyTOF, and TCRseq) using the package variancePartition/Dream on R (9). Covariates with less than 5% effect on the model were excluded from modeling. (RRID:SCR_001905, RRID:SCR_015654, RRID:SCR_006442)

Survival and Cox proportional hazard models. Univariable and multivariable regression models were used to estimate the hazard ratios (HRs) and corresponding 95% confidence intervals (CIs) for OS (Overall Survival) and PFS. Log rank and Gehan-Breslow tests were used to assess the significance of the difference between endpoints for OS and PFS. The univariable models were used to determine which covariates should be kept in the multivariable models. Significance was defined as adjusted p-values or False Discovery Rate (FDR) <0.05.

Adjust p-values for multiple comparisons. For multi-omic assays (Olink, Serology and CyTOF), we applied moderate T test statistics. We adjusted p-values using the Benjamini & Hochberg method (1995). This helps to control the false discovery rate, the expected proportion of false discoveries amongst the rejected hypotheses. Nonetheless, throughout the manuscript we show nominally significant results as $p<0.05$ and adjusted p values represented as $FDR<0.05$.

Differential expression. Differential protein expression analysis was performed in R using the packages Dream, lme4, from bioconductor. The mixed effect models were built using the covariates shown in Fig. 1B. For Olink the independent variables were individual protein levels (NPX). For CyTOF the independent variables were the surface markers 95 quantile values. The results were visualized using pheatmap and ggplot2 packages.

Differential abundance. We used the Limma-Dream-lme4 pipeline (9) in R to assess differential abundance between populations while modeling the covariates previously indicated in Fig.1B.

This approach was used for CyTOF and TCRseq. The clonal expansion populations were defined by Immunarch (10). T cell clones were classified into four groups: clones that had little evidence of expansion (unique/small clones/non expanded, 1e-5<x<=1e-4% of total clones), clones with some or medium expansion (1e-4<x<=0.001% of total clones), clones with large expansion (0.001<x<=0.01% of total clones) and hyperexpanded clones (0.01<x<=1% of total clones).

Correlation analyses. We used cor, corrplot, pvclust and hmisc packages in R-Stats to perform Pearson (linear) and Spearman (non-linear) correlations between analytes and endpoints.

Prediction of PFS using logistic regression. We used the package RMS and ROCR available on R to build classifiers of PFS status using the olink analytes as predictors and clinical variables as covariates. The internal validation was done using cross fold 5 validation.

Data availability statement

All data is available upon request at CIDC-CIMAC portal: https://cidc.nci.nih.gov/ upon request. All code used for analysis is available upon request at https://github.com/eegk. Data used to generate figures shown in this article are attached as supplementary table 2. Including data for Olink, CyTOF populations, Serology and TCR beta chain frequency.

Results

Three consecutive treatment groups (BV+I, BV+N, or BV+I+N) were enrolled, representing 54 patients with available biospecimens evaluable for correlative markers (Fig. 1A). Blood samples were collected before treatment (baseline), during cycle 2 (C2D1), during patient reevaluation (restaging), and after completion (off-study) to assess molecular and cellular baseline measurements and changes over time on all available PBMC and plasma samples (S. Table 1). We performed assay-specific quality control and variance profiling followed by a linear mixed-effect model to identify differential markers across time, treatments, and responses (Fig. 1B). This approach allows to minimize the effects of stage and tumor size (bulky disease) (20). Statistical significance was defined as false discovery rate (FDR) adjusted or unadjusted p-values.

DYNAMIC CHANGES IN PERIPHERAL BLOOD PLASMA SOLUBLE ANALYTES ASSOCIATED WITH TREATMENT BENEFIT

Soluble protein analyte profiles were measured using a standardized panel of 92 inflammation and immuno-oncology-related proteins (Olink) in all 54 patients with available longitudinal plasma samples (S. Table 1). First, we assessed significant changes from baseline related to treatment arms. Treatment with BV+I+N or BV+N led primarily to a durable increase in soluble PDCD1*/PD-1* levels, while BV+I induced increases from baseline for an array of T cell effector and cytotoxicity-associated markers such as IFN-γ, GZMA*, GZMH, CD27, CD28, and IL12RB1 (*FDR<0.05 or p<0.05) (Figs.1C-D and S Fig. 1). Treatments with BV+I also increased decoy and apoptotic markers CAIX*, PTN, MICA/B, Gal9, TRAIL (Fig. 1C and S Figs. 1), which was not observed after N-containing treatment. Conversely, levels of several circulating proteins associated with inflammation, including CCL17*, ANGPT2*, MMP12*, IL-13*, CXCL13*, CCL23, were high at baseline and showed a decrease over time associated with N-containing treatments, but less so with BV+I (Fig. 1C). In addition, T cell survival- and exhaustion-related cytokines (LAG3, TNFRSF4/OX40, CD8A, IL-7, IL-15, PD-L1) were decreased after nivolumab

use but not in BV+I (Fig. 1C). Overall, the largest change from baseline was observed for soluble PCDC1/PD-1 levels in N-containing therapy groups, attributed in part to drug interaction where nivolumab-bound PD-1 may be stabilized in circulation (Figs. 1C-D). Still, even in the absence of nivolumab (BV+I group), soluble PD-1 levels also increased from baseline to C2D1, suggesting immune activation.

Next, we asked whether soluble analytes differed per timepoint between responders and non-responders, using best overall response achieved. Out of 54 patients, 49 had evaluable clinical response data. Responders were defined as those experiencing CR or PR (n=43), while non-responders had SD or PD (n=6). Analysis of clinical outcomes associated with Olink data was assessed regardless of treatment group (BV+I, BV+N, BV+I+N) due to the low number of events per group. The levels of plasma CXCL13, CCL17, and VEGFA showed gradual decreases from baseline in responders while, conversely, they significantly increased in non-responders over time (Fig. 1E-F). Additionally, responders had lower ADA (adenosine-deaminase) and CD5 levels at baseline and stayed low throughout treatment, while non-responders had spikes in ADA and CD5 levels early on which normalized towards end of study (Figs. 1E-F).

To analyze the impact of soluble plasma analytes on clinical benefit, we performed univariate and multivariate Cox regression (adjusted for age, sex, tumor stage and treatment group) and Kaplan-Meier analyses of progression-free survival (PFS), using baseline Olink measurements. Progression-free survival benefit was associated individually with above median levels of VEGFR2 (Fig. 2A). Conversely, higher than median levels CXCL9 and MUC16 were associated with worse PFS (Figs. 2C & E). Multivariate Cox regression confirmed MUC16 association with worse hazard ratios, independently from age or sex or stage (Fig. 2F). However, CXCL9 and VEGFR2 only showed trends in multivariate Cox regression (Fig. 2B & D), potentially due to the effect of Ann Arbor Stage (Figs. B, D & F).

To understand better the prognostic capabilities of these markers, we built a PFS classifier using clinical variables alone and combined with VEGFR2, MUC16, or CXCL9 (Fig. 2G). The results showed that indeed adding any of these 3 markers could predict progression better than clinical variables alone. Also, they showed that area under the curve was the highest for VEGFR2 (0.75) followed by MUC16 (0.74), CXCL9 (0.73), PD-L1 (0.70) (selected as control) and clinical variables (0.68).

Next, we compared log rank test to Cox modeling in progression free survival (Fig. 2H), orthogonally verifying the results for VEGFR2, MUC16, and CXCL9. This approach was applied to overall survival revealing association of IL10, CCL19, VEGFR2, and TIE2 with better OS outcomes and CXCL10 and IFN-gamma with worst OS outcomes (Fig.2I). However, these findings were not reproduced in multivariate analysis (Supplementary table 3).

In summary, we found potentially prognostic 3 markers associated with PFS outcomes, but we did not find a significant association with treatment, making it difficult to distinguish their predictive vs. prognostic role.

DYNAMIC CHANGES IN PERIPHERAL BLOOD IMMUNE CELL SUBSETS ASSOCIATED WITH TREATMENT BENEFIT

Peripheral blood mononuclear cell (PMBC)-derived subpopulations were quantified using CyTOF from 51 patients with available cryopreserved biospecimens (S. Table 1). Differences in 30 immune cell subsets and 8 compartments (including a category for unidentified cells) were quantified simultaneously by semi-automated analysis using the Astrolabe and R platforms. The

predominant immune compartments in blood were T cells, followed by neutrophils, monocytes, and B Cells (Fig. 3A). Treatments with nivolumab led to an increase in plasmacytoid dendritic cells (pDC) in the bloodstream (FDR<0.05, Fig. 3B&E). Plasmablast B cells also showed a transient increase from baseline across all three therapy groups, with the most significant increase observed in BV+I after the initial treatment cycle (Figs. 3 B&C). Additionally, neutrophils and naïve $CD4^+$ T cells showed significant treatment-dependent but divergent changes from baseline, occurring in BV+N vs. other combinations (Fig. 3D&F). Specifically, naïve $CD4^+$ T cells decreased after one cycle of BV+I but increased at the end of BV+N, while neutrophils decreased after one cycle of BV+N but increased at the end of BV+I+N (Fig. 3D, F). When comparing treatment groups per timepoint, differences in cellular abundance were found at baseline in $CD14^+$ $CD16^+$ monocytes, neutrophils, CD4+ T_{EMRA} cells, and $CD56^+$ $CD16^+$ NK cells (Fig. 3G), pointing to potential imbalances prior to treatment in these non-randomized patients. Post-treatment memory B cells were significantly more abundant in BV+N vs. others, while neutrophils were more frequent in BV+I+N vs. others (Fig. 3H). Overall, nivolumab-containing regimens appeared to significantly raise levels of antigen-presenting cells (pDC, Fig 3E, H), while the triplet combination resulted in higher inflammatory cell subsets (neutrophils, Fig 3F, H).

DIFFERENTIAL EXPRESSIONS OF PERIPHERAL IMMUNE CELL SURFACE MARKERS ASSOCIATED WITH TREATMENT BENEFIT

PBMC subsets were also evaluated by CyTOF for inducible surface markers and changes in their expression. Durable decrease in PD-1 expression in various T cell subsets ($CD8^+$ & $CD4^+$) was seen after nivolumab treatments compared with BV+I (S Figs. 2A-B), attributed to known masking of epitope accessibility after nivolumab administration which prevents PD-1 detection during the assay, rather than to a biological observation. Reduced expression of other cell surface markers was associated with nivolumab treatments relative to ipilimumab, including HLA-DR (on memory B cells, $CD4^+$ $CD8^+$ T cells), CD45RA (on memory B cells), CD39 (on memory B cells, $CD27^-$ B cells), CD8 (on $CD56^+$ $CD16^+$ NK cells), CD57 (on $CD56^+$ CD16- NK cells, type 2 $CD1c^+$ dendritic cells), and CD95 (on $CD14^-$ $CD16^+$ monocytes) (S Figs. 2A-B).

When analyzing surface expression changes by response to treatment, CD56 and CD45 levels on NKT cells were found lower in non-responders at baseline (S Figs. 2C-D). Similarly, CD57 expression on $CD8^+$ T_{EMRA} started lower and increased in non-responders over time (S. Figs. 2C-D). Interestingly, pharmacodynamic changes post-treatment in CXCR3 expression on pDC showed higher expression in responders compared to non-responders (S. Figs. 2C-D). In summary, CXCR3 could be useful as an activation marker on pDC in responders, while T_{EMRA} expression of CD95 and CD57 was associated with resistance.

CIRCULATING ANTIBODIES TO TUMOR-ASSOCIATED ANTIGEN ASSOCIATED WITH TREATMENT BENEFIT

Autoantibody (AuAb) profiling of common tumor-associated antigens was performed in longitudinal plasma samples from all 54 patients using ELISA Grand Serology for IgG titers against a series of 19 full-length recombinant proteins (S. Table 1). At multiple time points in each therapy group, tumor-associated antibodies were detected in both responders and non-responders (Fig. 4A). NY-ESO-1 AuAbs were detected in more than 40 percent of patients who were non-responders, from baseline and at all four time points (Fig.4B). In comparison, though prevalent at baseline, NY-ESO-1 AuAbs were absent in more than 90 percent of responder patients after treatment initiation. Antibody titers for NY-ESO-1 were more often not detected

(negative) and had lower average titers in responders than non-responders at all time points (Fig. 4B).

T CELL CLONAL EXPANSION ASSOCIATION WITH TREATMENT BENEFIT

T cell clones derived from PBMCs TCR Vβ were classified into two groups: clones that had little evidence of expansion (unique/small clones/non-expanded, <=1e-4% of total clones) and clones with evidence of expansion (>1e-4%). We used two standardized metrics (clonal expansion and diversity) for investigating the association of clonality with treatment or response. There were no significant differences in clonal diversity over time except an increase in BV+N at restaging compared to baseline ($p<0.05$) (Fig. 4C). However, clonal overlap increased during treatment regardless of treatment type ($p<0.05$) (Fig. 4D). There was no significant difference between clonal expansion between BV+I+N, BV+N, and BV+I (Fig.4E). When looking at clinical benefit, the percentage of expanded clones was higher in responders vs. non-responders at C2D1 ($p<0.05$), but not at other time points (Fig. 4F). Finally, clonal diversity was increased in responders compared to non-responders at restaging and off-study, approached but did not reach statistical significance ($p>0.05$) (Fig. 4G). Overall, evidence of clonal expansion and clonal overlap following treatment was found, with marginal contribution to clinical benefit.

BIOMARKERS ASSOCIATION WITH ADVERSE EVENTS

Although variations in the number of adverse events (AEs) were reported among BV+I+N, BV+N, and BV+I treatments, our analysis did not reveal a significant association between AEs and biomarkers in any of the assays. We meticulously excluded unlikely related and unrelated AEs, focusing on grades 3 to 5 and dose-limiting toxicities with greatest clinical impact. The complexity of associating adverse events with biomarkers stems from intricate interactions involving genetic predispositions, environmental influences, and individual response variations.

Discussion

In this study, we examined peripheral molecular and cellular markers for their ability to distinguish differential treatment response and progression-free survival in patients with R/R HL treated with combination of single or dual checkpoint inhibitor combined with ADC (Suppl. Fig.3). Our findings contribute to the understanding of the immune landscape of HL using rigorously validated and harmonized multi-omics technological platforms for immune monitoring of novel therapies. The overarching goal of these research efforts was to identify potential immune signatures for risk stratification and therapeutic decision-making for patients with HL treated with immunotherapy (11). Soluble plasma or serum proteins have previously been reported as capable of distinguishing HL from healthy patients through immune response-related markers such as PD-L1, CCL17, CCL3, IL-13, MMP12, TNFRS4, and LAG3 (12). We found proteins that increased in plasma post-treatment, particularly enriched in cytotoxicity-related markers (IFN-γ, GZMA/H, CD244) following treatment with I-containing arms, while decreases in stromal-derived factors, such as CCL17, ANGPT2, IL13, CXCL13 were observed in N-containing arms. Interestingly, higher levels of CCL17, as well as ADA, CXCL13, CD5, and VEGFA, were associated with lack of treatment response, regardless of treatment type. Some of these proteins have been previously associated with adverse HL outcome: CCL17 from tumors, also known as TARC (13,14), CXCL13 in PD-1+ T cells (15); VEGF in tumors (16,17). Further, elevated levels of these proteins have been linked to HL compared to healthy controls (18). Despite constitutive expression of PD-L1 in HL and reports of serum PD-L1 as a potential

predictor of response (19-21), we did not observe soluble PD-L1 as a clinically relevant marker in plasma. Interestingly, the strongest markers of progression were ADA and CD5, which were transiently elevated early post-treatment (C2D1) in non-responders. Though these markers had not been previously shown as prognostic in HL, there is literature showing ADA and its ligand CD26 as higher in ALK-positive NHL and HL (22) as well as being associated with poor outcome in other tumor types (23).

Importantly, despite high CR rates, many patients recur and therefore, PFS may be a better prognostic marker of durable benefit. We identified elevated plasma CXCL9 and MUC16 at baseline, and reduced VEGFR2 as associated with worse PFS. MUC16, also known as CA125, has been extensively described as a marker associated with progression in solid tumors (24), but it is underexplored in HL. The amount of soluble VEGFR2 may be contributing to how much ligand is available for tumor growth and vascularization. It is also not clear why CXCL9 levels, which increase with immunotherapy, had a negative impact on PFS, but it could reflect patients with higher prior lines of treatment, since CXCL9 levels are affected by prior immunotherapies, or represent higher baseline inflammation, which has been described to be a poor predictor (25). Lymphoma cytogenetic features, including tumor mutation burden, could also affect the analytes measured in blood, but unfortunately, data from tumor tissue was not available for our analysis at the current time. Overall, our study validates previous studies and suggests novel soluble proteins associated with treatment resistance.

Although the potential role of $CD4^+$ T cells as inflammatory/immune regulators in HL has previously been associated with response (26,27), we found no changes in effector or regulatory $CD4^+$ T cells except $CD4^+$ T_{EMRA} and NK cells differentially prevalent at baseline across treatment groups. Additionally, increased B memory cells and neutrophils were associated with treatment (highest in BV+I+N), both of which have been associated with refractory disease (27). Interestingly, plasmacytoid dendritic cells were generally highly increased with all treatments and CXCR3 induction on pDC was associated with favorable response to treatment. While pDC are generally rare, they are usually reliably identified due to their distinct lineage markers. Because CXCR3-ligands CXCL9 and CXCL10 were detected in circulation of patients with poor survival, we speculate that they may reduce CXCR3 pDC from circulation due to homing to tissues. In contrast, CXCR3 pDC in blood would be expected to be more prevalent with low CXCL9/10. The data may indicate pDC have a pathogenic role in HL, as has been previously observed with increased circulating pDCs with favorable response to treatment of HL (28).

Patients with resistance to treatment also had increased levels of surface markers CD56 on NKT, CD57 and CD95 on $CD8^+$ T_{EMRA}, that may indicate improper differentiation of effectors. CD57 has been associated with terminal differentiation and senescence of NK cells, and our data suggests the expansion of this phenotype over time in non-responders. While provocative, these observations require prospective validation (29-32). T cell clonal expansion is widely reported as a prognostic signature of response in patients with HL (33,34), specifically when associated with the expansion of $CD4^+$ T cells or gamma delta T cells (35). Patients with clonally expanded T cells at baseline confirmed some of these observations, and we also observed trends of increase in clonal diversity over time, although it did not reach statistical significance potentially due patient heterogeneity.

Our study also investigated the impact of tumor-specific autoantibody (AuAb) profiles on drug mechanisms and outcomes. NY-ESO-1, MAGEA4, PRAME, and SSX2 are potential cancer-testis antigens that have been associated with HL in various studies and tested in clinical trials

(36). Evidence in solid tumors suggests that patients with NY-ESO-1 preexisting immunity fare better than NY-ESO-1 seronegative patients after checkpoint blockade (37). Here, we observed the opposite, where non-responders were enriched in NY-ESO-1 Ab at baseline (Fig. 4A), even though a small fraction (<15%) of responders also showed the presence of NY-ESO-1 AuAb (Fig. 4B). Like other cancer-testis antigens, NY-ESO-1 expression in cancer is induced by DNA hypomethylation and histone acetylation (38). Antibodies could therefore be a surrogate for more aggressive tumors, which we could not confirm due to absence of tissues to correlate antigen presence. While past studies have failed to link clinical benefit to expression of these cancer-testis antigens in HL (39), more recent attempts at harnessing T cell response via adoptive transfer have demonstrated safety and preliminary efficacy of targeting cancer-testis antigens (40). Therefore, considering the role of endogenous immunity using cancer-related plasma circulating AuAb could be useful and would be warranted in future studies.

Important limitations of this study include absence of available tumor tissues to investigate the source or impact of peripheral markers on the tumor microenvironment. In addition, it is important to note that patients were not randomly assigned to treatment groups, and that attrition of available samples occurred with time. Nevertheless, the statistical modeling strategy used allows minimization of these biases by incorporating fixed and random effects. Additionally, the large imbalance in responders vs. non-responders precluded treatment-specific analyses of clinical benefit, which were only evaluated for the entire cohort. Finally, we could not properly quantify neutrophil counts, known to be prognostic in HL, because cellular assays were conducted with PBMCs, though qualitative differences could still be assessed in neutrophils surviving density gradient purification.

In summary, we found that elevated circulating plasma proteins CXCL13, ADA, CXCL9, MUC16 and CCL17 as well as NY-ESO-1 autoantibodies were associated with poor outcomes to treatment with BV combined with I, N, or both. Together, it is possible that elevated baseline levels of plasma CXCL9, presence of tumor-related NY-ESO-1 autoantibodies, and reduced plasma VEGFR2 highlight heavily pre-treated tumors that may exhibit primary resistance to treatment despite presumed presence of immune infiltration and recognition. In addition, markers increasing from baseline in patients progressing through treatment include CXCL13, CCL17, and reduced clonal T cell diversity, likely reflecting increasing tumor burden and activation of a Tfh axis previously associated with poor prognosis of lymphocyte-rich HL (41). Reduced cytotoxicity-related markers on NKT and T_{EMRA} were also seen at start of treatment in patients with poor outcomes, while increases in circulating CXCR3 pDCs were associated with favorable response, as also observed independently (28). These results suggest drug-related mechanistic effects on immune cell activity that could contribute to treatment sensitivity or response vs. resistance, and potentially impact treatment decision making. If validated these findings may also suggest novel therapeutic strategies. The phase 2 component of this clinical trial (NCT01896999) has concluded enrollment, and we will prospectively validate the immune markers identified in this study. If validated, these may be important tools towards a personalized approach to immunotherapy in HL.

Acknowledgments

We thank the patients and their families for participating in the study. We thank Beatriz Sanchez-Espiridion and Julia Mendoza Perez for their assistance with sample procurement and inventory, Rebecca Enos from the Emmes Company, LLC, for organizational and administrative support. We thank Dr. Yasuko Tada and Nishikawa (National Cancer Center, Japan) for their gift of several recombinant proteins used in the ELISA. We thank the patients and their families for participating in the study. The study was performed under the aegis of the Cancer Immune Monitoring and Analysis Centers and Cancer Immunologic Data Commons (CIMAC-CIDC) Network, which was established with support of the Cancer Moonshot^{SM} Initiative of the National Cancer Institute (42). We acknowledge and warmly thank the following members of the Division of Cancer Treatment & Diagnosis: program directors Magdalena Thurin and Minkyung Song, associate branch chief Helen X. Chen, and Howard Streicher as the lead reviewer and drug monitor, for their roles in the selection, coordination, and supervision of this study as part of the CIMAC-CIDC network. We also thank Jennifer Grant Lee for her support writing the initial version of the article in her capacity as FNIH-sponsored medical writer.

Financial Support

Scientific and financial support for the CIMAC-CIDC Network is provided through the National Cancer Institute (NCI) Cooperative Agreements U24CA224319 (to the Icahn School of Medicine at Mount Sinai CIMAC), U24CA224331 (to the Dana-Farber Cancer Institute CIMAC), U24CA224285 (to the MD Anderson Cancer Center CIMAC) and U24CA224316 (to the CIDC at Dana-Farber Cancer Institute). ECOG-ACRIN study E4412 was supported in part by NIH/NCI grants CA224319. S.G. was additionally supported by grants U01DK124165 and P30CA196521. This study was coordinated in part by the ECOG-ACRIN Cancer Research Group (Peter J. O'Dwyer, MD and Mitchell D. Schnall, MD, PhD, Group Co-Chairs) and supported by the National Cancer Institute of the National Institutes of Health under award numbers: U10CA180820, U10CA180794, UG1CA233339, and UG1CA232760. The content is solely the responsibility of the authors and does not necessarily represent the official views of the National Institutes of Health. This work was supported in part through the computational and data resources and staff expertise provided by Scientific Computing and Data at the Icahn School of Medicine at Mount Sinai and supported by the Clinical and Translational Science Award (CTSA) grant UL1TR004419 from the National Center for Advancing Translational Sciences.

Author contribution statement

EGK, CD & SG conceptualized the project, designed the study, supervised, and oversaw the project, analyzed data, and wrote the manuscript. EGK, HHH, OJ & SG Performed analysis, contributed to writing and reviewing the article. DMDV, SG & SKS, managed sample collection and transfer. VB, KT, GK, MP, HX, JH, KA, KN performed the assay work and reviewed the article. RM, JA, DYD, BSK, SMA, JY, EC, JL, IIW, SKS provided critical feedback and facilitated regulatory work associated with the clinical data.

References

1. Younes A, Gopal AK, Smith SE, Ansell SM, Rosenblatt JD, Savage KJ*, et al.* Results of a pivotal phase II study of brentuximab vedotin for patients with relapsed or refractory Hodgkin's lymphoma. J Clin Oncol 2012;30:2183-9
2. Armand P, Engert A, Younes A, Fanale M, Santoro A, Zinzani PL*, et al.* Nivolumab for Relapsed/Refractory Classic Hodgkin Lymphoma After Failure of Autologous Hematopoietic Cell Transplantation: Extended Follow-Up of the Multicohort Single-Arm Phase II CheckMate 205 Trial. J Clin Oncol 2018;36:1428-39
3. Kamat S, Patel J, Brown BR, Vyas A. Adverse Events Induced by Nivolumab Plus Ipilimumab vs. Nivolumab Monotherapy among Cancer Patients: A Systematic Review and Meta-Analysis. Cancer Invest 2022;40:777-88
4. De Silva P, Aiello M, Gu-Trantien C, Migliori E, Willard-Gallo K, Solinas C. Targeting CTLA-4 in cancer: Is it the ideal companion for PD-1 blockade immunotherapy combinations? Int J Cancer 2021;149:31-41
5. Diefenbach CS, Hong F, Ambinder RF, Cohen JB, Robertson MJ, David KA*, et al.* Ipilimumab, nivolumab, and brentuximab vedotin combination therapies in patients with relapsed or refractory Hodgkin lymphoma: phase 1 results of an open-label, multicentre, phase 1/2 trial. Lancet Haematol 2020;7:e660-e70
6. Germain C, Gnjatic S, Tamzalit F, Knockaert S, Remark R, Goc J*, et al.* Presence of B cells in tertiary lymphoid structures is associated with a protective immunity in patients with lung cancer. Am J Respir Crit Care Med 2014;189:832-44
7. Gnjatic S, Old LJ, Chen YT. Autoantibodies against cancer antigens. Methods Mol Biol 2009;520:11-9
8. Sahaf B, Pichavant M, Lee BH, Duault C, Thrash EM, Davila M*, et al.* Immune Profiling Mass Cytometry Assay Harmonization: Multicenter Experience from CIMAC-CIDC. Clin Cancer Res 2021;27:5062-71
9. Hoffman GE, Roussos P. Dream: powerful differential expression analysis for repeated measures designs. Bioinformatics 2021;37:192-201
10. Nazarov V, Tsvetkov V, Fiadziushchanka S, Rumynskiy E, Popov A, Balashov I*, et al.* immunarch: bioinformatics analysis of T-cell and B-cell immune repertoires. 2023:https://immunarch.com/, https://github.com/immunomind/immunarch
11. Mottok A, Steidl C. Biology of classical Hodgkin lymphoma: implications for prognosis and novel therapies. Blood 2018;131:1654-65
12. Gholiha AR, Hollander P, Lof L, Larsson A, Hashemi J, Ulfstedt JM*, et al.* Immune-Proteome Profiling in Classical Hodgkin Lymphoma Tumor Diagnostic Tissue. Cancers (Basel) 2021;14:9
13. Zijtregtop EAM, Diez C, Zwaan CM, Veening MA, Beishuizen A, Meyer-Wentrup FAG. Thymus and activation-regulated chemokine (TARC) as treatment response marker for paediatric Hodgkin lymphoma: A pilot study. Br J Haematol 2023;200:70-8
14. Viviani S, Mazzocchi A, Pavoni C, Taverna F, Rossi A, Patti C*, et al.* Early serum TARC reduction predicts prognosis in advanced-stage Hodgkin lymphoma patients treated with a PET-adapted strategy. Hematol Oncol 2020;38:501-8
15. Aoki T, Chong LC, Takata K, Milne K, Marshall A, Chavez EA*, et al.* Single-cell profiling reveals the importance of CXCL13/CXCR5 axis biology in lymphocyte-rich classic Hodgkin lymphoma. Proc Natl Acad Sci U S A 2021;118:e2105822118

16. Yang J, Li W, He X, Zhang G, Yue L, Chai Y. VEGF overexpression is a valuable prognostic factor for non-Hodgkin's lymphoma evidence from a systemic meta-analysis. Dis Markers 2015;2015:786790
17. Koh YW, Han JH, Yoon DH, Suh C, Huh J. PD-L1 expression correlates with VEGF and microvessel density in patients with uniformly treated classical Hodgkin lymphoma. Ann Hematol 2017;96:1883-90
18. Ma Y, Visser L, Roelofsen H, de Vries M, Diepstra A, van Imhoff G*, et al.* Proteomics analysis of Hodgkin lymphoma: identification of new players involved in the cross-talk between HRS cells and infiltrating lymphocytes. Blood 2008;111:2339-46
19. Veldman J, Alsada ZND, van den Berg A, Plattel WJ, Diepstra A, Visser L. Soluble PD-L1 is a promising disease biomarker but does not reflect tissue expression in classic Hodgkin lymphoma. Br J Haematol 2021;193:506-14
20. De Re V, Caggiari L, Repetto O, Mussolin L, Mascarin M. Classical Hodgkin's Lymphoma in the Era of Immune Checkpoint Inhibition. J Clin Med 2019;8:1596
21. Ribas A, Wolchok JD. Cancer immunotherapy using checkpoint blockade. Science 2018;359:1350-5
22. Kameoka J, Ichinohasama R, Inoue H, Yamamoto J, Yokoyama H, Tomiya Y*, et al.* CD26, together with cell surface adenosine deaminase, is selectively expressed on ALK-positive, but not on ALK-negative, anaplastic large cell lymphoma and Hodgkin's lymphoma. Leuk Lymphoma 2006;47:2181-8
23. Gao ZW, Yang L, Liu C, Wang X, Guo WT, Zhang HZ*, et al.* Distinct Roles of Adenosine Deaminase Isoenzymes ADA1 and ADA2: A Pan-Cancer Analysis. Front Immunol 2022;13:903461
24. Aithal A, Rauth S, Kshirsagar P, Shah A, Lakshmanan I, Junker WM*, et al.* MUC16 as a novel target for cancer therapy. Expert Opin Ther Targets 2018;22:675-86
25. Mulder TA, Andersson ML, Pena-Perez L, Heimersson K, Xagoraris I, Wahlin BE*, et al.* Immune Biomarkers in the Peripheral Blood and Tumor Microenvironment of Classical Hodgkin Lymphoma Patients in Relation to Tumor Burden and Response to Treatment. Hemasphere 2022;6:e794
26. Cader FZ, Schackmann RCJ, Hu X, Wienand K, Redd R, Chapuy B*, et al.* Mass cytometry of Hodgkin lymphoma reveals a CD4(+) regulatory T-cell-rich and exhausted T-effector microenvironment. Blood 2018;132:825-36
27. Cader FZ, Hu X, Goh WL, Wienand K, Ouyang J, Mandato E*, et al.* A peripheral immune signature of responsiveness to PD-1 blockade in patients with classical Hodgkin lymphoma. Nat Med 2020;26:1468-79
28. Galati D, Zanotta S, Corazzelli G, Bruzzese D, Capobianco G, Morelli E*, et al.* Circulating dendritic cells deficiencies as a new biomarker in classical Hodgkin lymphoma. Br J Haematol 2019;184:594-604
29. Herrera AF, Palmer J, Adhikarla V, Yamauchi D, Poku EK, Bading J*, et al.* Anti-CD25 radioimmunotherapy with BEAM autologous hematopoietic cell transplantation conditioning in Hodgkin lymphoma. Blood Adv 2021;5:5300-11
30. Matou-Nasri S, Rabhan Z, Al-Baijan H, Al-Eidi H, Yahya WB, Al Abdulrahman A*, et al.* CD95-mediated apoptosis in Burkitt's lymphoma B-cells is associated with Pim-1 down-regulation. Biochim Biophys Acta Mol Basis Dis 2017;1863:239-52
31. Maaland AF, Saidi A, Torgue J, Heyerdahl H, Stallons TAR, Kolstad A*, et al.* Targeted alpha therapy for chronic lymphocytic leukaemia and non-Hodgkin's lymphoma with the anti-CD37 radioimmunoconjugate 212Pb-NNV003. PLoS One 2020;15:e0230526

32. Yuan CT, Chuang SS, Cheng PY, Chang K, Wang H, Tsai JH*, et al.* Decreased CD11c-positive dendritic cells in the tumor microenvironment predict double-hit/triple-hit genotype and survival in diffuse large B-cell lymphoma. J Pathol Clin Res 2022;8:436-47
33. Mussolin L, Damm-Welk C, Pillon M, Woessmann W. Minimal Disease Monitoring in Pediatric Non-Hodgkin's Lymphoma: Current Clinical Application and Future Challenges. Cancers (Basel) 2021;13:1907
34. Wartewig T, Kurgyis Z, Keppler S, Pechloff K, Hameister E, Ollinger R*, et al.* PD-1 is a haploinsufficient suppressor of T cell lymphomagenesis. Nature 2017;552:121-5
35. Muller CKS, Spagnuolo J, Audige A, Chancellor A, Russenberger D, Scherrer AU*, et al.* Immunophenotypic characterization of TCR gammadelta T cells and MAIT cells in HIV-infected individuals developing Hodgkin's lymphoma. Infect Agent Cancer 2021;16:24
36. Thomas R, Al-Khadairi G, Roelands J, Hendrickx W, Dermime S, Bedognetti D*, et al.* NY-ESO-1 Based Immunotherapy of Cancer: Current Perspectives. Front Immunol 2018;9:947
37. Yuan J, Adamow M, Ginsberg BA, Rasalan TS, Ritter E, Gallardo HF*, et al.* Integrated NY-ESO-1 antibody and CD8+ T-cell responses correlate with clinical benefit in advanced melanoma patients treated with ipilimumab. Proc Natl Acad Sci U S A 2011;108:16723-8
38. Oi S, Natsume A, Ito M, Kondo Y, Shimato S, Maeda Y*, et al.* Synergistic induction of NY-ESO-1 antigen expression by a novel histone deacetylase inhibitor, valproic acid, with 5-aza-2'-deoxycytidine in glioma cells. J Neurooncol 2009;92:15-22
39. Chen YT, Chadburn A, Lee P, Hsu M, Ritter E, Chiu A*, et al.* Expression of cancer testis antigen CT45 in classical Hodgkin lymphoma and other B-cell lymphomas. Proc Natl Acad Sci U S A 2010;107:3093-8
40. Vasileiou S, Lulla PD, Tzannou I, Watanabe A, Kuvalekar M, Callejas WL*, et al.* T-Cell Therapy for Lymphoma Using Nonengineered Multiantigen-Targeted T Cells Is Safe and Produces Durable Clinical Effects. J Clin Oncol 2021;39:1415-25
41. Aoki T, Chong LC, Takata K, Milne K, Marshall A, Chavez EA*, et al.* Single-cell profiling reveals the importance of CXCL13/CXCR5 axis biology in lymphocyte-rich classic Hodgkin lymphoma. Proc Natl Acad Sci U S A 2021;118:e2105822118
42. Chen HX, Song M, Maecker HT, Gnjatic S, Patton D, Lee JJ*, et al.* Network for Biomarker Immunoprofiling for Cancer Immunotherapy: Cancer Immune Monitoring and Analysis Centers and Cancer Immunologic Data Commons (CIMAC-CIDC). Clin Cancer Res 2021;27:5038-48

Figure legends

Figure 1. Protein dynamics in Hodgkin lymphoma during checkpoint blockade treatment. **A.** Overview of the clinical trial E4412 experimental design. Three treatment arms included: (1) Brentuximab vedotin (BV) + ipilimumab (I); (2) BV + nivolumab (N); and (3) BV+I+N, with participant number (n) indicated. **B.** Regression modeling strategy using mixed effect models applied to analyze independently four different assay methodologies. Each assay was modeled considering relevant clinical variables and adjusted for multiple testing using false discovery rate (FDR) correction. **C.** Summary heatmap showing the log2-fold change (Log2FC) between time points and treatments. The changes with a positive Log2FC over time in color blue are associated with a decrease over time and red with an increase over time. The –log10(p-value) is represented by the size of the circles, indicating statistical significance as the circles increase. **D.** Line and boxplot figures showing the changes in expression for markers increased post treatment such as PDCD1, GMZA, PTN, CAIX, IL18, CD28 and markers decreased post

treatment such as CCL17, ANGPT2, IL13 and CXCL13. **E.** Summary heatmap of differential expression associated with response. The changes with a positive Log2FC in color blue are associated with a lower expression in non-responders and red with higher expression in non-responders. **F.** Line and boxplot examples of significant ($p<0.05$ & $FDR<0.05$) proteins associated with response (blue) or non-response (red) over time.

Figure 2. Association of plasma cytokines with clinical benefit. A, C & E. PFS survival analysis shows the Kaplan Meyer curves for VEGFR2, CXCL9 and MUC16, respectively. Statistics using log rank test and cox proportional hazard models are shown. Higher than median VEGFR2 levels were associated with slower progression while higher than median levels of CXCL9 and MUC16 were associated with faster progression. **B, D & F**. Forest plot for VEGFR2, CXCL9 and MUC16, respectively. Here, we show the multivariate statistics for each of these proteins including sex, age, treatment type, and cancer stage (Ann Arbor stage). These figures verify the directionality of the KM curves showed and show that these 3 proteins are independent of these clinically relevant covariates. **G.** Shows the Receiver operating characteristic (ROC) curves for the prediction of PFS using VEGFR2, MUC16, CXCL9, PD-L1 and clinical variables. Ordered from most relevant to least relevant model, reflected on the AUC values. **H.** Univariate PFS Cox modeling of Olink analytes. **I.** Univariate OS Cox modeling of Olink analytes. Both I and H, show in the x-axis the hazard ratio and the y-axis shows the -log10(p-values) based on the log rank test.

Figure 3. Cellular dynamics in Hodgkin lymphoma during checkpoint blockade treatment. A. Cell type composition of major cell groups (myeloid and lymphoid) for all available samples at baseline. This bar plot shows the composition and variation of cellular components, including unassigned cells, across all patients. The cell types were identified using a semi-automated approach with the software Astrolabe. **B.** Heatmap map showing differentially abundant cell type changes over time. The rows are shown as relative abundance or scaled (z-score) allowing comparison across samples for each cell type simultaneously. **C-F.** Boxplots and line plots colored based on treatment showing the dynamics for the differentially abundant cell types. **G.** Boxplots showing the differentially abundant cells between treatments at baseline. **H.** Comparison of cell abundances for different treatments after the start of treatment.

Fig. 4. Cancer antigen detection and T cell clonal dynamics associated with treatment and response. A. Heatmap showing cancer antigen detection by ELISA for all samples. The color represents the log10 scale antibody titers. Positive detection is considered above levels of 2 (pink), while negative detection is represented by the color black. The top rows of the figure show the treatment group, best overall response, and time. The figure is separated into non-responders (left) and responders (right). Each column box is hierarchically clustered for simplicity. **B.** Pie charts showing the association of NY-ESO-1 presence (left column) and non-detection (middle column). Boxplots (right column) show all titer levels for non-responders and responders. **C.** Boxplots showing the standardized absolute clonal diversity index calculated using Immunarch R package. The clonal diversity are changes are shown over four time points (Baseline, C2D1, Restaging, and Off study) per treatment arm. The p-value from Wilcoxon rank test is shown on top of the boxes. The y-axis is identical for all 3 treatment arms. There was no statistical difference between the treatments due the observed large variances (patient heterogeneity). **D.** Boxplots showing increase in clonal overlap over time for all 3 treatments. P values were estimated using Wilcoxon ranked test. **E.** Clonal expansion was stratified into unique and expanded clones (black and orange, respectively). The stacked barplot shows the average percent of each clonal expansion class over time and per treatment arm. There were

no statistical differences identified between treatment arms. **F.** Boxplots showing the percent abundance of only expanded clones shown for responders and non-responders over time. There were no significant differences between these two groups except for C2D1 using Wilcoxon rank test. **G.** Clonal diversity boxplots comparing responders and non-responders. Overall, responders had a higher diversity yet, it did not reach statistical significance.

Figure 1.

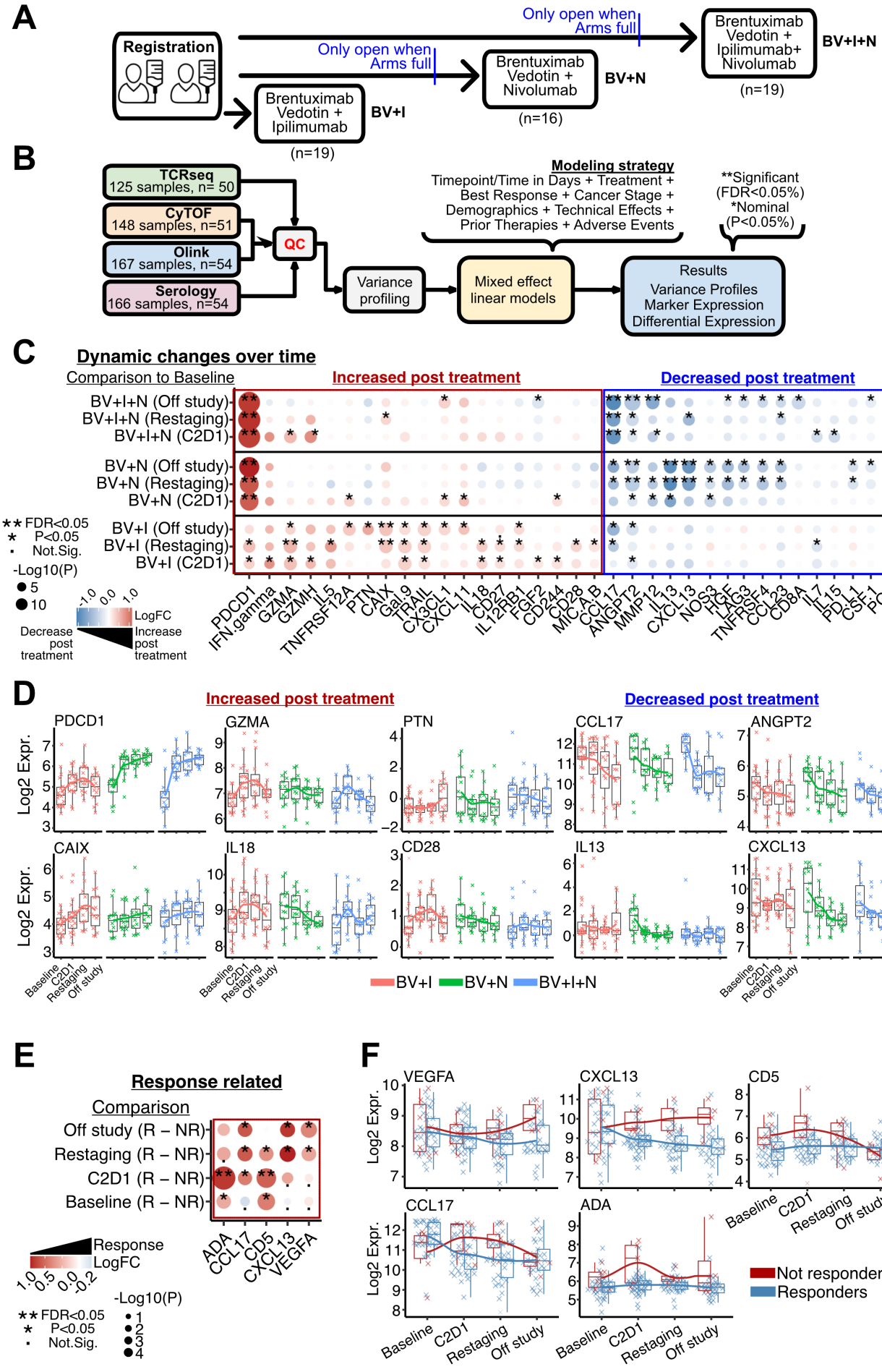

Figure 2

A

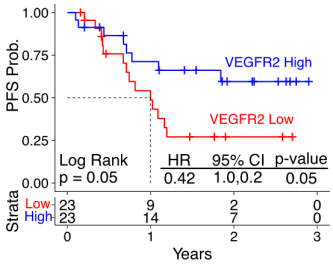

B

VEGFR2 Multivariate Cox Regression with variance driving covariates

Variable		N	Hazard ratio	p
VEGFR2	High	23	Reference	
	Low	23	1.60 (0.56, 4.56)	0.38
Treatment	BV+I	19	Reference	
	BV+I+N	14	0.62 (0.18, 2.12)	0.45
	BV+N	13	0.36 (0.11, 1.19)	0.09
Sex	Female	23	Reference	
	Male	23	1.09 (0.37, 3.27)	0.87
Age		46	1.01 (0.96, 1.07)	0.68
Ann Arbor Stage	I	2	Reference	
	II	21	0.67 (0.06, 7.49)	0.74
	III	13	1.96 (0.19, 20.46)	0.57
	IV	10	2.22 (0.14, 34.17)	0.57

C

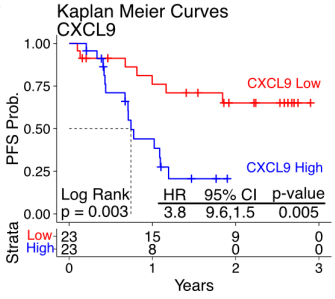

D

CXCL9 Multivariate Cox Regression with variance driving covariates

Variable		N	Hazard ratio	p
CXCL9	High	23	Reference	
	Low	23	0.44 (0.13, 1.46)	0.2
Treatment	BV+I	19	Reference	
	BV+I+N	14	0.70 (0.21, 2.32)	0.6
	BV+N	13	0.40 (0.12, 1.32)	0.1
Sex	Female	23	Reference	
	Male	23	0.87 (0.28, 2.71)	0.8
Age		46	1.01 (0.96, 1.07)	0.7
Ann Arbor Stage	I	2	Reference	
	II	21	0.58 (0.05, 6.56)	0.7
	III	13	1.56 (0.14, 17.37)	0.7
	IV	10	1.47 (0.08, 25.92)	0.8

E

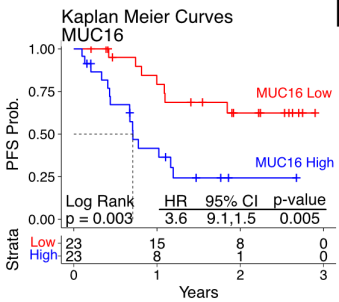

F

MUC16 Multivariate Cox Regression with variance driving covariates

Variable		N	Hazard ratio	p
MUC16	High	23	Reference	
	Low	23	0.29 (0.09, 0.86)	0.03
Treatment	BV+I	19	Reference	
	BV+I+N	14	0.90 (0.26, 3.12)	0.87
	BV+N	13	0.54 (0.16, 1.79)	0.31
Sex	Female	23	Reference	
	Male	23	0.90 (0.28, 2.86)	0.86
Age		46	1.03 (0.97, 1.09)	0.38
Ann Arbor Stage	I	2	Reference	
	II	21	0.49 (0.04, 5.57)	0.56
	III	13	1.13 (0.10, 12.88)	0.92
	IV	10	1.74 (0.13, 23.66)	0.68

G

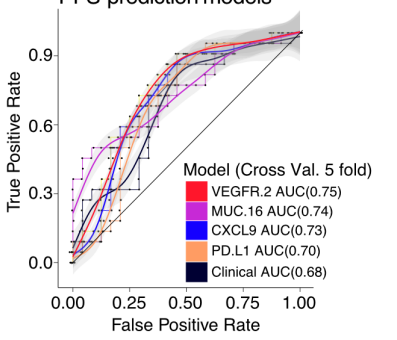

H

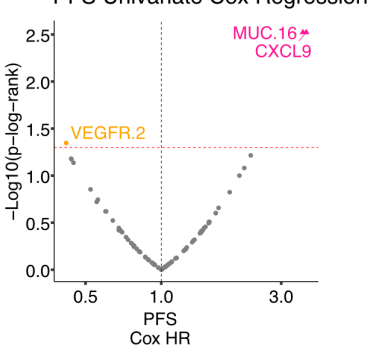

I

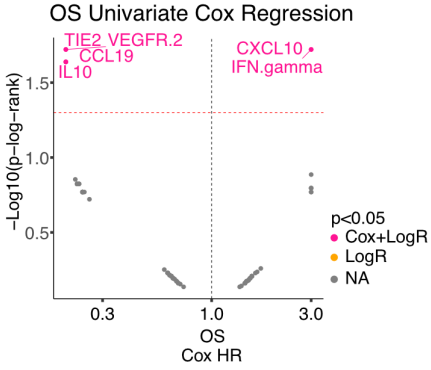

Figure 3

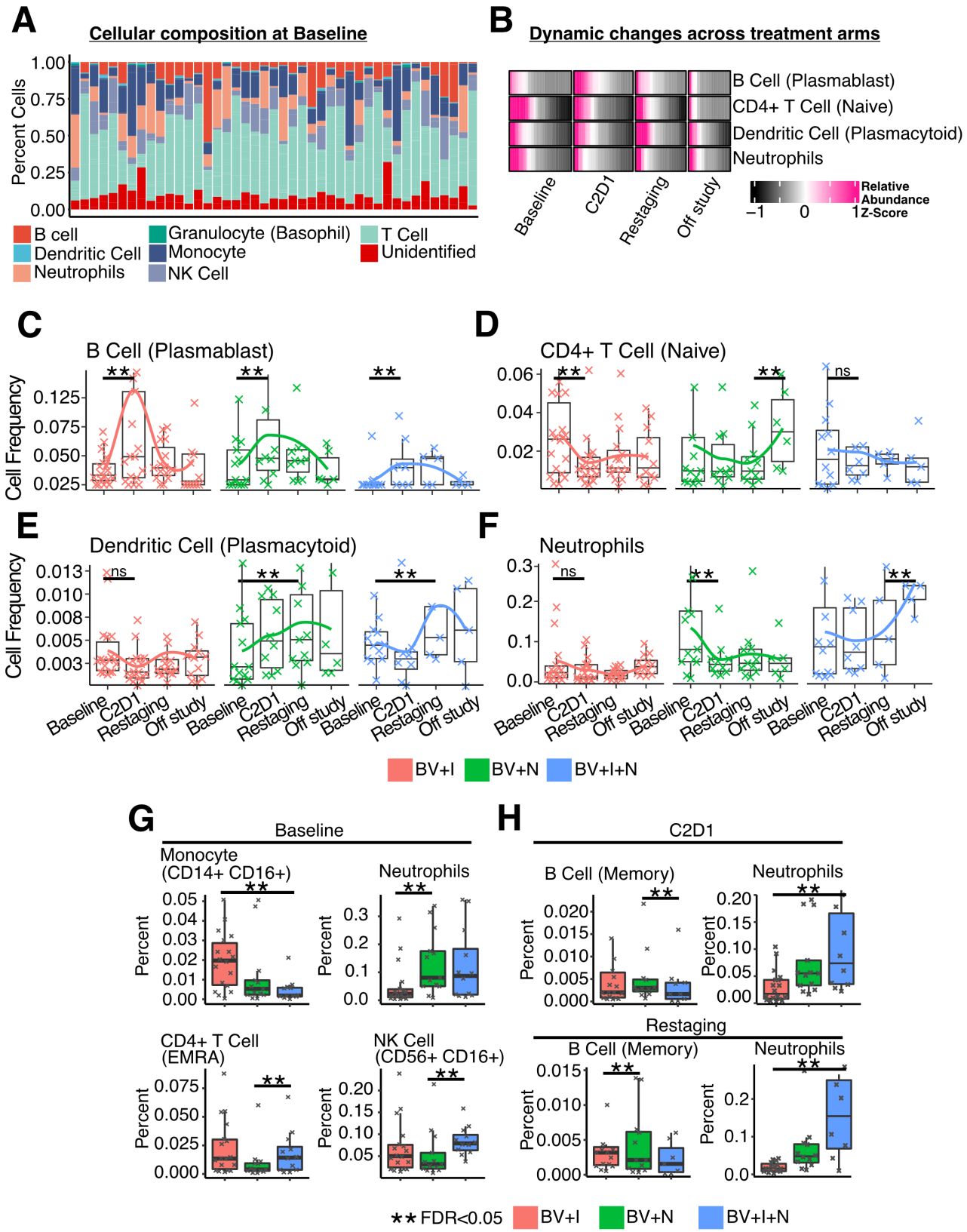

Figure 4